Chu-Fang Chou,[1] Yi-Yu Lin,[1] Hsu-Kun Wang,[1] Xiaolin Zhu,[2] Matteo Giovarelli,[3] Paola Briata,[3] Roberto Gherzi,[3] W. Timothy Garvey,[2] and Ching-Yi Chen[1]

KSRP Ablation Enhances Brown Fat Gene Program in White Adipose Tissue Through Reduced miR-150 Expression

Diabetes 2014;63:2949–2961 | DOI: 10.2337/db13-1901

Brown adipose tissue oxidizes chemical energy for heat generation and energy expenditure. Promoting brown-like transformation in white adipose tissue (WAT) is a promising strategy for combating obesity. Here, we find that targeted deletion of KH-type splicing regulatory protein (KSRP), an RNA-binding protein that regulates gene expression at multiple levels, causes a reduction in body adiposity. The expression of brown fat–selective genes is increased in subcutaneous/inguinal WAT (iWAT) of *Ksrp*$^{-/-}$ mice because of the elevated expression of PR domain containing 16 and peroxisome proliferator–activated receptor gamma coactivator 1α, which are key regulators promoting the brown fat gene program. The expression of microRNA (miR)-150 in iWAT is decreased due to impaired primary miR-150 processing in the absence of KSRP. We show that miR-150 directly targets and represses *Prdm16* and *Ppargc1a*, and that forced expression of miR-150 attenuates the elevated expression of brown fat genes caused by KSRP deletion. This study reveals the in vivo function of KSRP in controlling brown-like transformation of iWAT through post-transcriptional regulation of miR-150 expression.

Obesity, caused by positive energy balance leading to expansion of adipocyte mass, increases the risk of diabetes, heart disease, and some forms of cancer. There are two major types of adipose tissues in mammals: white adipose tissue (WAT) and brown adipose tissue (BAT). WAT is the main storage site of excess energy, primarily in the form of triacylglycerol (TG). Conversely, BAT is specialized to dissipate chemical energy for heat generation primarily through uncoupling protein 1 (UCP1). UCP1 uncouples mitochondrial electron transport from ATP synthesis by permeabilizing the inner mitochondrial membrane to allow intermembrane protons to leak back into the mitochondrial matrix (1). The activity of BAT inversely correlates with BMI in adult humans (2,3). Promoting BAT function has a potential to defend against obesity and obesity-associated disorders (4). A distinct type of UCP1-positive adipocytes, designated as beige or brite (brown-in-white) cells, is found sporadically in WAT of adult animals upon exposure to long-term cold or β-adrenergic agonists (5–7). This brown-like transformation of WAT is most prominent in the inguinal subcutaneous depot, whereas epididymal/perigonadal adipose tissue is less susceptible to browning (8), the formation of multilocular UCP1-positive adipocytes. The emergence of these inducible brown-like adipocytes is associated with a protection against obesity and metabolic diseases in rodent models (8–11).

Classic brown adipocytes develop from Myf5-positive precursors through the action of transcriptional regulators PR domain containing 16 (PRDM16) and CCAAT/enhancer binding protein-β (12,13). However, the inducible brown-like adipocytes arise from a non-Myf5 cell lineage. The browning of WAT in rodents can be induced by hormones

[1]Department of Biochemistry and Molecular Genetics, University of Alabama at Birmingham, Birmingham, AL
[2]Department of Nutrition Sciences, University of Alabama at Birmingham, Birmingham, AL
[3]Gene Expression Regulation Laboratory, Istituto Nazionale per la Ricerca sul Cancro, Genova, Italy
Corresponding authors: W. Timothy Garvey, garveyt@uab.edu, and Ching-Yi Chen, cchen@uab.edu.

Received 17 December 2013 and accepted 4 April 2014.
This article contains Supplementary Data online at http://diabetes.diabetesjournals.org/lookup/suppl/doi:10.2337/db13-1901/-/DC1.

such as irisin (14) and FGF12 (15), pharmacological activation of peroxisome proliferator–activated receptor (PPAR)-γ (16), and modulation through various transcriptional regulators including PRDM16 (8), PPARGC1α/PPARγ coactivator 1α (17), forkhead box class C2 (9), receptor interacting protein 140 (10,18), transcription intermediary factor 2 (19), pRb, and p107 (20,21). Recently, several microRNAs (miRNAs) were shown to regulate brown fat differentiation and brown-like transformation of WAT. miRNA (miR)-133 inhibits brown adipocyte differentiation by directly repressing *Prdm16* expression (22), and also regulates the choice between myogenic and brown adipose determination using multipotent adult skeletal muscle stem cells (satellite cells) that can give rise to both myogenic and brown adipogenic lineages (23). miR-196a is essential for brown adipogenesis of white fat progenitor cells by repressing the expression of Hoxc8 (24). miR-193b and miR-365 are essential for brown fat differentiation by repressing myogenesis as well as by promoting brown adipogenesis (25). miR-155 inhibits brown and beige adipocyte differentiation by repressing CCAAT/enhancer binding protein-β (26).

KH-type splicing regulatory protein (KSRP) is a multifunctional RNA-binding protein involved in post-transcriptional regulation of gene expression. This includes splicing (27), mRNA decay (28), primary miRNA (pri-miRNA) processing (29), and translation (30). KSRP binds the AU-rich elements in the 3′ untranslated regions (UTRs) of inherently unstable mRNAs and promotes their decay by recruiting mRNA decay machineries (28,31). KSRP also interacts with the terminal loops of a subset of miRNA precursors and promotes their maturation in cultured cells (29). However, the in vivo function of KSRP in controlling mRNA decay and pri-miRNA processing, and the associated phenotypes resulting from KSRP deficiency have not been completely established. To do this, we have generated *Ksrp*-null mice (32). In the current study, we report that $Ksrp^{-/-}$ mice exhibit decreased fat mass owing to a reduction in TG content. The expression of brown fat–selective and fatty acid oxidation genes is increased in WAT in the absence of KSRP. We also find that high-fat feeding upregulates miR-150 and KSRP in inguinal WAT (iWAT) and the deletion of KSRP significantly decreases adiposity in diet-induced obesity (DIO). Thus, these findings establish KSRP and miR-150 as important regulators for brown-like transformation of iWAT and whole-body adiposity.

RESEARCH DESIGN AND METHODS

Animal Studies

The generation of *Ksrp*-null mice on a C57BL/6J congenic background has been described (32). Mice were maintained under a 12-h light/dark cycle at a room temperature of 22°C and were fed a normal chow diet (NCD) or a high-fat diet (HFD) containing 45% kcal from fat (Harlan Laboratories). All experiments were performed using 10- to 16-week-old, age-matched, wild-type and $Ksrp^{-/-}$ male mice, which were littermate offspring of $Ksrp^{+/-} \times Ksrp^{+/-}$. For metabolic analysis, including food intake, activity, and indirect calorimetry, mice were individually housed. Food intake and physical activity were measured using the Comprehensive Lab Animal Monitoring System. VO_2 and VCO_2 were measured by indirect calorimetry. Energy expenditure (EE) was calculated using the equation of $EE = (3.941 \times VO_2) + (1.106 \times VCO_2)$ and normalized with respect to lean mass. Body fat content and lean mass were measured by dual-energy X-ray absorptiometry. All animal studies were conducted in accordance with guidelines for animal use and care established by the University of Alabama at Birmingham Animal Resource Program and the Institutional Animal Care and Use Committee.

Measurement of Adipocyte Number, Adipocyte Size, and TG Content

Adipocytes were isolated from epididymal and inguinal fat depots by collagenase digestion as described previously (33). The floating adipocytes were collected and washed with Krebs-Ringer HEPES buffer. Adipocyte number and size were determined as described previously (34). Briefly, aliquots of evenly suspended isolated adipocytes were removed for optical sizing of cell diameter with ImageJ (National Institutes of Health) using a micrometer ruler as a reference for the diameter and for determination of the volume occupied by packed adipocytes using microhematocrit capillary tubes. Adipocyte number was derived by dividing the volume occupied by packed adipocytes with the mean adipocyte volume obtained by optical sizing of the diameter. Lipids were extracted from adipocytes in 1% Triton X-100, and TG content was determined using Infinity reagent (Thermo Scientific).

mRNA Analysis

Total RNA was extracted by TRIzol (Invitrogen). For quantitative real-time RT-PCR analysis, total RNA (1 μg) was reverse transcribed using a mixture of oligo(dT) and random hexamers. Amplification was performed by using an LightCycler 480 and the SYBR Green system (Roche). mRNA levels were normalized to that of β-actin or cyclophilin B mRNAs. The primer sequences are listed in Supplementary Table 1.

miRNA Microarrays and Analysis

RNA was isolated from iWATs of six wild-type and six $Ksrp^{-/-}$ mice by miRNeasy (Qiagen). Individual RNA of wild-type mice and individual RNA of $Ksrp^{-/-}$ mice were pooled together, respectively, and subjected to genome-wide miRNA microarray analysis in triplicate, which was performed by Phalanx Biotech. The miRNAs whose signals were fivefold above the background signal (these miRNAs are arbitrarily considered to be expressed in the iWAT) and were elevated by more than twofold in the $Ksrp^{-/-}$ iWAT were selected for further analysis. For miRNA expression analysis, total RNA was converted into cDNA by miScript II RT Kit (Qiagen) and was subjected to real-time PCR with a specific primer for miR-150 using miScript Primer Assay (Qiagen). miRNA levels were normalized to that of U6 small nuclear RNA.

miRNA Target Prediction

miRNA target prediction was performed by using the miRWalk database (http://www.umm.uni-heidelberg.de/apps/zmf/mirwalk/).

pri-miRNA In Vitro Processing Assays

pri-miRNA processing assays were performed as described previously (29,35). Briefly, a DNA template producing pri-miR-150 was generated by PCR. ^{32}P-labeled pri-miR-150 was synthesized by in vitro transcription and incubated with total extracts of wild-type and *Ksrp*$^{-/-}$ iWATs in a processing buffer containing 100 mmol/L KCH_3COOH, 2 mmol/L Mg $(CH_3COOH)_2$, 10 mmol/L Tris-Cl (pH 7.6), 2 mmol/L dithiothreitol, 10 mmol/L creatine phosphate, 1 μg of creatine phosphokinase, 1 mmol/L ATP, 0.4 mmol/L guanosine triphosphate, 0.1 mmol/L spermine, and 2 units of RNasin at 37°C. RNA was isolated and subjected to 10% polyacrylamide-urea gel electrophoresis and autoradiography.

Ribonucleoprotein Immunoprecipitation Assays

Ribonucleoprotein immunoprecipitation assays were performed as described previously (35,36). Briefly, cell lysates were immunoprecipitated with Dynabeads (Invitrogen) coated with protein A/protein G and coupled with anti-KSRP serum at 4°C overnight. Pellets were washed four times, and RNA was isolated from the immunocomplexes using miRNeasy, reverse transcribed, and amplified by quantitative PCR (qPCR).

Immunoblotting and Antibodies

Cells or tissues were lysed in radioimmunoprecipitation assay buffer (0.5% NP-40, 0.5% sodium deoxycholate, 0.1% SDS, 150 mmol/L NaCl, 50 mmol/L Tris-Cl, pH 7.5). Proteins were separated using 7–10% SDS-PAGE, transferred to a polyvinylidene fluoride membrane, and probed with the following antibodies: anti-PRDM16 (R&D Systems), anti-PPARGC1α (Abcam), anti-PPARα (Santa Cruz Biotechnology), anti-KSRP (37), anti-UCP1 (Abcam), anti-β-actin (Abcam), and anti-α-tubulin (Sigma-Aldrich).

Immunohistochemistry of UCP1

Paraffin-embedded sections were incubated with anti-UCP1 antibodies (1:500; Abcam), followed by detection using the Vectastain ABC Kit (Vector Laboratories).

Isolation, Differentiation, and Transfection of Stromal-Vascular Fraction Cells

Stromal-vascular fraction (SVF) cells were prepared from iWAT as described previously (33), cultured in DMEM/F12 containing 10% FBS, and induced for differentiation by incubating confluent cells with DMEM/F12 medium containing 10% FBS, 5 mg/mL insulin, 0.5 mmol/L isobutylmethylxanthine, 1 μmol/L dexamethasone, 1 nmol/L triiodothyronine (T3), 125 nmol/L indomethacin, and 1 μmol/L rosiglitazone for 48 h. Cells were maintained in maintenance medium containing 10% FBS, 1 nmol/L T3, and 1 μmol/L rosiglitazone. The medium was replaced every 2 days. For transfection of SVF cells, 80–90% of confluent cells were transfected with miRNA mimics (50 nmol/L), miRNA inhibitors (100 nmol/L), or small interfering RNAs (siRNAs) (60 nmol/L) using HiPerFect (Qiagen). The transfected cells were induced for differentiation the following day and collected for analysis 5 days postinduction.

Measurement of Oxygen Consumption Rates

SVF cells were seeded (15,000 cells/well) in XF24 culture microplates (Seahorse Bioscience) and induced for differentiation. At day 5 of differentiation, the oxygen consumption rate (OCR) was measured using an XF24 analyzer. Basal respiration was assessed in untreated cells, and uncoupled respiration was assessed after the addition of 10 μmol/L oligomycin. Nonmitochondrial respiration was measured after the addition of 4 μmol/L antimycin A and 1 μmol/L rotenone.

Luciferase Reporters and Assays

Dual luciferase reporters, expressing firefly luciferase containing the 3′ UTRs of *Prdm16* and *Ppargc1a*, and *Renilla* luciferase, were purchased from GeneCopoeia. A control reporter, pEZX-MT01, was also purchased from GeneCopoeia. The predicted miR-150 target sites were mutated by PCR-mediated site-directed mutagenesis, and mutations were confirmed by DNA sequencing. NIH3T3 cells were transfected with 1 μg of a reporter together with an miRNA mimic (50 nmol/L) using Lipofectamine (Invitrogen). Cells were collected 36–48 h after transfection, and luciferase activities were measured using the Luc-Pair miR Luciferase Assay Kit (GeneCopoeia). Firefly luciferase activity was normalized to internal control *Renilla* luciferase activity.

miRNA Mimics, miRNA Inhibitors, and siRNAs

miR-150 mimic and inhibitor were purchased from Qiagen. siGENOME SMARTpool siRNAs against *Prdm16* and *Ppargc1a* were purchased from Thermo Scientific. Control miRNA mimic and inhibitor and a control siRNA were purchased from Qiagen.

Statistical Analysis

All data are presented as the mean ± SEM. Comparisons between two groups were performed using an unpaired two-tailed Student *t* test. One-way ANOVA, followed by Fisher least significant difference test, was used for multiple comparisons.

RESULTS

Ksrp$^{-/-}$ Mice Exhibit Reduced Adiposity

Ksrp$^{-/-}$ mice were lean with a 10% reduction in body weight in males eating a NCD compared with wild-type littermates (Fig. 1*A*) resulting from a reduction in the mass of distinct fat pads (Fig. 1*B*). A similar reduction in body weight and fat mass was also observed in female *Ksrp*$^{-/-}$ mice (Supplementary Fig. 1*A* and *B*). By contrast, no significant difference in the weights of organs, such as liver, spleen, kidney, and heart, was detected between the two groups (Supplementary Fig. 1*C*). Consistent with these findings, body composition analysis showed a reduction in whole-body fat mass, but not in lean mass, in *Ksrp*$^{-/-}$ mice (Supplementary Fig. 1*D* and *E*).

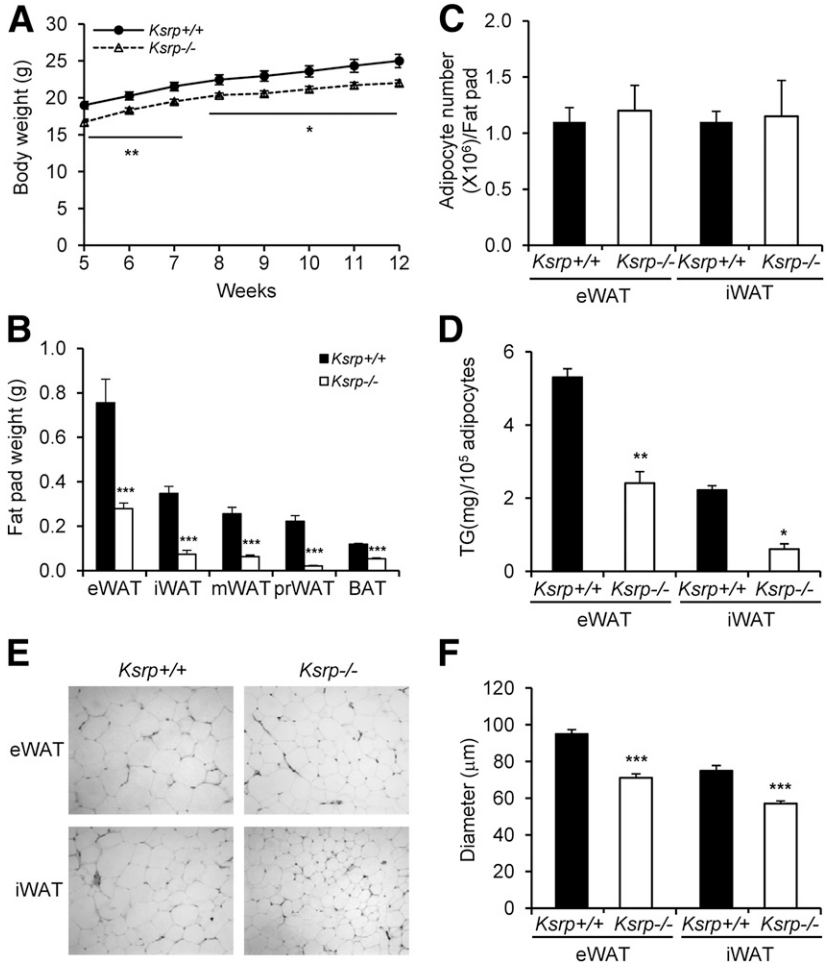

Figure 1—KSRP ablation causes a reduction in body weight, fat pad weight, TG content, and adipocyte size, but not adipocyte number. *A*: Body weights of wild-type (n = 8) and $Ksrp^{-/-}$ male mice (n = 8) from week 5 to week 12. *B*: Fat pad weights of 14-week-old wild-type (n = 8) and $Ksrp^{-/-}$ (n = 8) male mice. mWAT, mesenteric WAT; prWAT, perirenal WAT. Number (*C*) and TG content (*D*) of adipocytes isolated from the eWAT and iWAT of 12-week-old wild-type (n = 4) and $Ksrp^{-/-}$ (n = 4) mice. *E*: Hematoxylin-eosin staining of paraffin-embedded sections of the eWAT and iWAT of wild-type and $Ksrp^{-/-}$ mice. *F*: Average diameters of adipocytes determined by optical sizing. Results were obtained from four wild-type and four $Ksrp^{-/-}$ mice, and ~100 adipocytes/mouse. All data are represented as the mean ± SEM. $^{*}P < 0.05$, $^{**}P < 0.01$, $^{***}P < 0.001$.

Reduction in adipose tissue mass can result from less TG storage, impaired adipocyte differentiation, or both. We isolated primary adipocytes from epididymal WAT (eWAT) and iWAT, and determined the adipocyte number and total TG content. While no difference in adipocyte number was observed (Fig. 1*C*), TG content was significantly reduced in $Ksrp^{-/-}$ eWAT and iWAT (Fig. 1*D*). Consistent with a decrease in TG content, adipocytes of $Ksrp^{-/-}$ eWAT and iWAT were smaller in size, as revealed by histological analysis (Fig. 1*E*), and there was a 25% decrease in the mean diameter of adipocytes in both the eWAT and iWAT of $Ksrp^{-/-}$ mice (Fig. 1*F*).

To further examine the cause of reduced fat mass, we subjected wild-type and $Ksrp^{-/-}$ mice to metabolic studies. No significant difference in food consumption and locomotor activity was observed between groups during the light and dark periods (Supplementary Fig. 1*F* and *G*). However, $Ksrp^{-/-}$ mice exhibited a moderate increase in EE as measured by indirect calorimetry during the dark period (Supplementary Fig. 1*H*). Collectively, these data suggest that the reduced adiposity in $Ksrp^{-/-}$ mice results from a reduction in TG content in WAT partly due to increased EE, but not reduced food consumption or increased activity.

Enhanced Expression of Brown Fat–Selective Genes in $Ksrp^{-/-}$ iWAT

To determine the molecular mechanism leading to reduced adiposity in $Ksrp^{-/-}$ mice, we examined the expression of genes involved in adipocyte differentiation and lipid metabolism in WAT. The expression of *Pparg*, but not of *Cebpa*, was moderately elevated in $Ksrp^{-/-}$ eWAT, and the expression of both *Cebpa* and *Pparg* was increased in $Ksrp^{-/-}$ iWAT (Supplementary Fig. 2*A*). There was no difference in the expression of adipocyte makers such as fatty acid

binding protein 4 (*Fabp4*) and perilipin 1 in either eWAT or iWAT between the two groups (Supplementary Fig. 2*A*). We examined the expression of genes involved in the pathways of TG synthesis (*Gpam*, *Agpat2*, *Agpat6*, and *Dgat2*), fatty acid synthesis (*Fasn*, *Acaca/Acc1*, and *Scd1*), and fatty acid uptake (*Lpl*, *Cd36*, and *Fatp1*). While no significant difference in their expression was observed in *Ksrp*$^{-/-}$ eWAT, the expression of these genes, except for *Dgat2*, *Lpl*, *Cd36*, and *Fatp1*, was significantly increased in *Ksrp*$^{-/-}$ iWAT (Supplementary Fig. 2*B–D*). These results suggest that KSRP ablation increases the expression of *Cebpa*, *Pparg*, and most of the genes involved in TG synthesis and de novo fatty acid synthesis in iWAT. However, the elevated expression of these genes is not consistent with a reduction in TG content in the WAT of *Ksrp*$^{-/-}$ mice.

We also observed that genes selectively expressed in BAT, including *Ucp1*, *Cidea*, *Cox8b*, and *Dio2*, were significantly upregulated in the iWAT of *Ksrp*$^{-/-}$ mice (Fig. 2*A*). The fold increase in brown fat–selective genes was much higher than that of TG synthesis and fatty acid synthesis genes (compare Fig. 2*A* with Supplementary Fig. 2). The expression of some brown fat genes was also moderately increased in *Ksrp*$^{-/-}$ eWAT, although their expression was much less than that in iWAT (Fig. 2*A*). In addition to brown fat markers, the expression of genes encoding brown fat transcriptional regulators, including *Ppargc1a* and *Ppara*, but not *Prdm16*, was also elevated in the iWAT and eWAT of *Ksrp*$^{-/-}$ mice (Fig. 2*B*). By contrast, no difference in the expression of these genes was observed between wild-type BAT and *Ksrp*$^{-/-}$ BAT (Supplementary Fig. 3*A* and *B*). The lack of an alteration in brown fat gene expression in *Ksrp*$^{-/-}$ BAT is likely due to a lower KSRP expression in BAT compared with iWAT (Supplementary Fig. 3*C*). Protein levels of PRDM16 (while *Prdm16* mRNA was not elevated), PPARGC1α, and PPARα were significantly increased in *Ksrp*$^{-/-}$ iWAT (Fig. 2*C*). Consistent with the elevated expression of PPARGC1α and PPARα, important regulators of fatty acid oxidation, the expression of *Cpt1b*, *Acadm*, and *Acadl* was also significantly increased in *Ksrp*$^{-/-}$ iWAT and eWAT (Fig. 2*D*). We also detected elevated levels of UCP1 protein and increased numbers of UCP1-positive adipocytes in *Ksrp*$^{-/-}$ iWAT, which contained clusters of multilocular cells (Supplementary Fig. 4*A* and *B*). Thus, the deletion of KSRP leads to brown-like transformation of iWAT that is characterized by the enhanced expression of brown fat–selective and fatty acid oxidation genes.

Decreased miR-150 Expression in *Ksrp*$^{-/-}$ iWAT Due to Impaired pri-mRNA Processing

KSRP regulates the maturation of some miRNAs by facilitating pri-miRNA processing. To determine whether the impaired expression of miRNAs plays a role in enhancing brown fat gene expression in *Ksrp*$^{-/-}$ iWAT, we subjected RNA samples to miRNA microarray analysis and only selected miRNAs whose expression was reduced in the absence of KSRP. We identified only one miRNA, miR-150, whose expression was reduced by more than twofold in *Ksrp*$^{-/-}$ iWAT (data not shown; see RESEARCH DESIGN AND METHODS). The expression of miR-150 was higher in the iWAT than in the eWAT and BAT of wild-type mice, and there was a threefold reduction in *Ksrp*$^{-/-}$ iWAT (Fig. 3*A*). Conversely, pri-miR-150 levels in *Ksrp*$^{-/-}$ iWAT were higher than that in wild-type iWAT (Fig. 3*B*), suggesting that the reduction in miR-150 levels was likely due to impaired pri-mR-150 processing. To determine the role of KSRP in pri-miR-150 processing, we performed ribonucleoprotein immunoprecipitation assays and observed that KSRP physically associated with pri-miR-150 in wild-type iWAT extracts (Fig. 3*C*). In contrast, pri-miR-34a was not associated with KSRP (Fig. 3*C*). The residual signals of pri-miR-34a in the anti-KSRP immunoprecipitates were likely due to a nonspecific interaction of anti-KSRP serum with pri-miR-34a. We carried out in vitro pri-miRNA processing assays and found that production of pre-miR-150 was significantly reduced using the cell lysate of *Ksrp*$^{-/-}$ iWAT (Fig. 3*D*). The addition of recombinant KSRP to *Ksrp*$^{-/-}$ lysate restored pre-miR-150 production (Fig. 3*E*). By contrast, processing of a control pri-miR-23b was equivalent between wild-type and *Ksrp*$^{-/-}$ lysates (Fig. 3*F*). These data indicate that decreased miR-150 expression in *Ksrp*$^{-/-}$ iWAT is indeed due to a reduction in pri-miR-150 processing.

Enhanced Brown Fat–Selective Gene Expression and Reduced miR-150 Expression in Differentiated SVF Cells of *Ksrp*$^{-/-}$ iWAT

To determine whether the increased brown-like transformation is cell autonomous, we isolated SVF cells of iWAT that are able to express brown fat–selective genes upon differentiation to adipocytes (8). After differentiation, the expression of *Ucp1*, *Cidea*, *Cox8b*, *Ppargc1a*, and *Ppara*, but not of *Prdm16*, was elevated in *Ksrp*$^{-/-}$ SVF cells (Fig. 4*A* and *B*). By contrast, no difference in the expression of adipocyte markers common to white and brown adipocytes, such as *Fabp4* and *Adipoq*, and a brown adipocyte–selective marker, *Elovl3*, was detected between wild-type and *Ksrp*$^{-/-}$ SVF cells (Fig. 4*C*). The expression of PRDM16, PPARGC1α, and PPARα was elevated in differentiated *Ksrp*$^{-/-}$ SVF cells (Fig. 4*D*). We examined miR-150 expression and observed a fivefold increase upon differentiation of wild-type SVF cells; we also observed that this increase was completely blunted in *Ksrp*$^{-/-}$ SVF cells (Fig. 4*E*). Furthermore, pri-miR-150 levels were decreased in differentiated wild-type SVF cells, but those levels were not altered in differentiated *Ksrp*$^{-/-}$ SVF cells compared with undifferentiated cells (Fig. 4*E*). These data indicate that the induction of miR-150 upon adipocyte differentiation occurs primarily through pri-miR-150 processing due to an increase in KSRP levels (Fig. 4*D*), and that the elevated expression of brown fat–selective genes and decreased miR-150

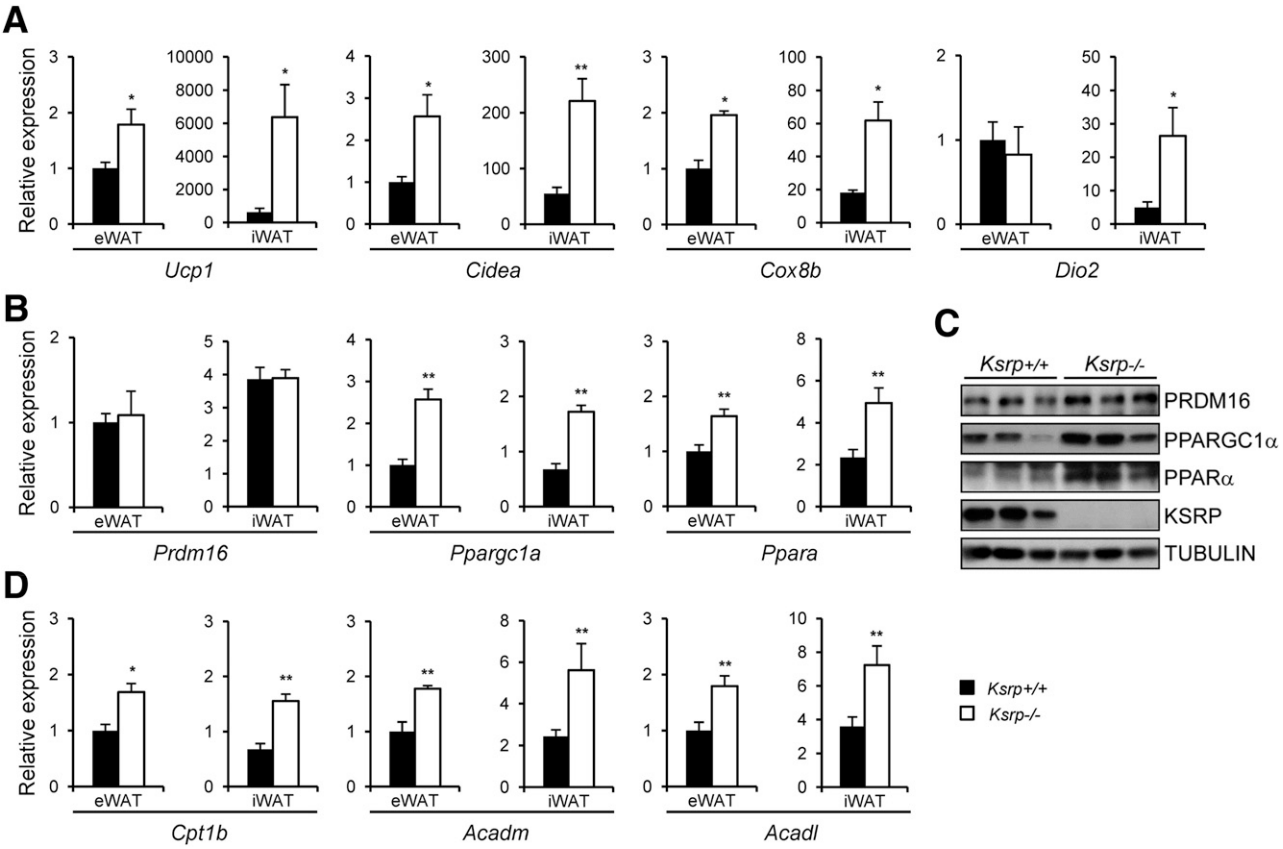

Figure 2—KSRP ablation elevates the expression of brown fat–selective genes, genes encoding brown fat transcriptional regulators, and genes involved in fatty acid oxidation in WAT. *A*: Expression of brown fat–selective genes, including *Ucp1*, *Cidea*, *Cox8b*, and *Dio2*, analyzed by qPCR in the eWAT and iWAT of wild-type ($n = 8$) and *Ksrp*$^{-/-}$ ($n = 8$) mice. The expression level of each gene in wild-type eWAT was set at 1. *B*: Expression of genes encoding brown fat transcriptional regulators, including *Prdm16*, *Ppargc1a*, and *Ppara*, analyzed by qPCR in the eWAT and iWAT of wild-type ($n = 8$) and *Ksrp*$^{-/-}$ ($n = 8$) mice. *C*: Immunoblot analysis of iWAT extracts of wild-type and *Ksrp*$^{-/-}$ mice using antibodies against PRDM16, PPARGC1α, PPARα, KSRP, and α-tubulin. *D*: Expression of fatty acid oxidation genes, including *Cpt1b*, *Acadm*, and *Acadl*, analyzed by qPCR in the eWAT and iWAT of wild-type ($n = 8$) and *Ksrp*$^{-/-}$ ($n = 8$) mice. All data are represented as the mean ± SEM. $^*P < 0.05$, $^{**}P < 0.01$.

expression in the absence of KSRP can be reproduced in adipocytes derived from SVF cells of iWAT.

miR-150 Negatively Regulates Expression of *Prdm16* and *Ppargc1a* and Mitochondrial Aspiration of Differentiated SVF Cells of *Ksrp*$^{-/-}$ iWAT

Target prediction analysis indicated that *Prdm16* and *Ppargc1a* are targets of miR-150. To determine the molecular mechanism leading to enhanced expression of brown fat genes and whether it is due to a reduction in miR-150 expression, we manipulated miR-150 levels in SVF cells of iWAT. The inhibition of miR-150 expression in wild-type SVF cells increased mRNA levels of *Ucp1*, *Cidea*, *Cox8b*, *Ppargc1a*, and *Ppara*, but not of *Prdm16* (Fig. 5*A* and *B*). Conversely, ectopic miR-150 expression in *Ksrp*$^{-/-}$ SVF cells markedly repressed the expression of *Ucp1*, *Cidea*, *Cox8b*, *Ppargc1a*, and *Ppara*, but not of *Prdm16* (Fig. 5*A* and *B*). By contrast, neither reduction nor overexpression of miR-150 changed the expression of *Fabp4* and *Adipoq* (Fig. 5*C*). The inhibition of miR-150 expression in wild-type SVF cells moderately enhanced the expression of PRDM16 and PPARGC1α, and, conversely, the overexpression of miR-150 in *Ksrp*$^{-/-}$ SVF cells caused a marked decrease in the protein levels (Fig. 5*D*).

To correlate the brown fat gene program with mitochondrial functions, we examined mitochondrial aspiration in differentiated SVF cells. *Ksrp*$^{-/-}$ adipocytes exhibited higher OCRs for basal and uncoupled (treated with oligomycin) aspirations, but not for nonmitochondrial aspiration (treated with antimycin A and rotenone), than wild-type adipocytes (Fig. 5*E*, left panel). Importantly, the treatment of *Ksrp*$^{-/-}$ adipocytes with a miR-150 mimic decreased basal and uncoupled aspirations (Fig. 5*E*, right panel). These data indicate that KSRP deficiency increases mitochondrial respiration activity because of reduced miR-150 expression.

To demonstrate that miR-150 can directly target *Prdm16* and *Ppargc1a* mRNAs, we cloned their 3′ UTRs into a dual luciferase reporter. We subcloned two overlapping fragments from each 3′ UTR owing to their large size (>3.5 kb). Fragment (F) 2 of *Prdm16* contains

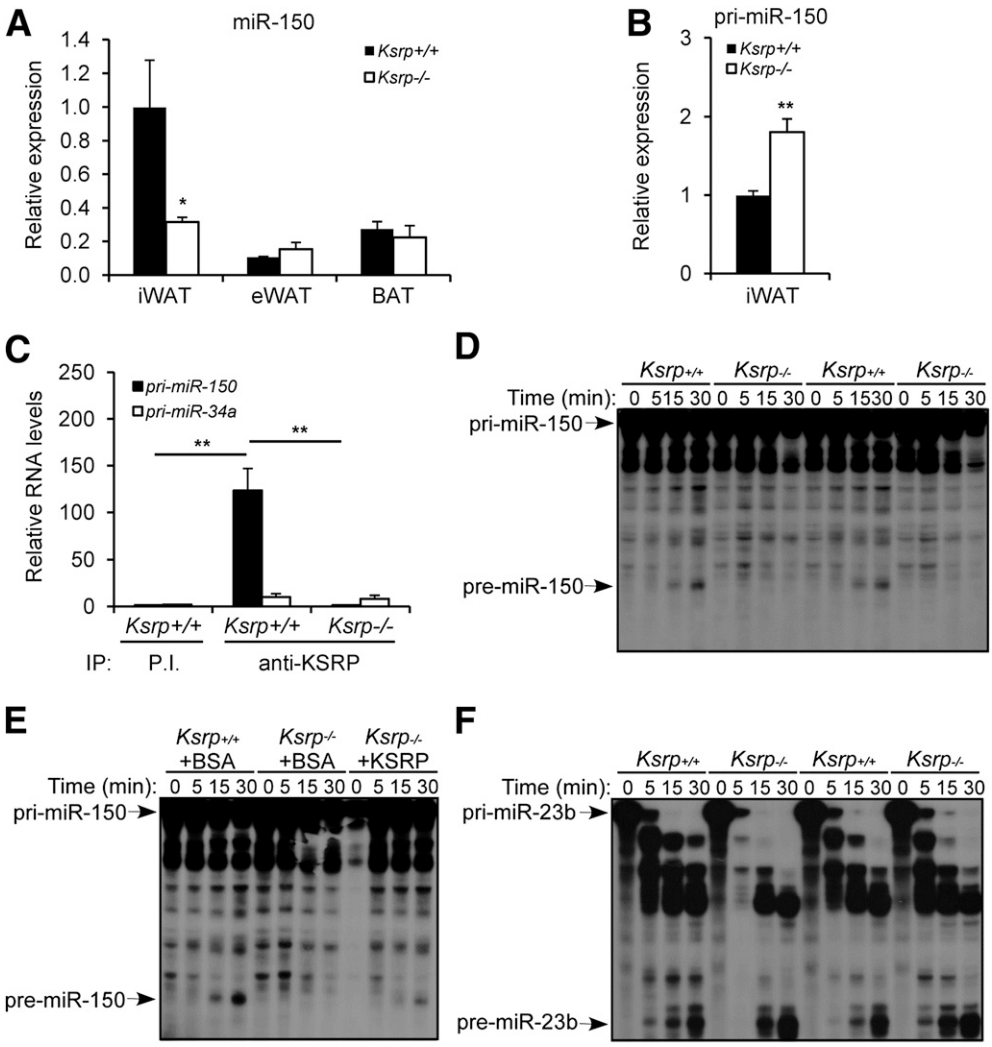

Figure 3—Decreased miR-150 expression in *Ksrp*$^{-/-}$ iWAT resulting from impaired pri-miR-150 processing. *A*: miR-150 levels analyzed by qPCR in eWAT, iWAT, and BAT of wild-type (n = 8) and *Ksrp*$^{-/-}$ (n = 8) mice. *B*: pri-miR-150 levels analyzed by qPCR in the iWAT of wild-type (n = 8) and *Ksrp*$^{-/-}$ (n = 8) mice. All data are represented as the mean ± SEM. *P < 0.05, **P < 0.01. *C*: Association of pri-miR-150 with KSRP. Extracts of wild-type and *Ksrp*$^{-/-}$ iWATs were immunoprecipitated with a control serum or anti-KSRP serum and anti-KSRP serum, respectively. pri-miR-150 and pri-miR-34a transcripts in the precipitates were analyzed by qPCR. Data are represented as the mean ± SEM of three independent experiments. **P < 0.01. IP, immunoprecipitation; P.I., preimmune serum. *D*: In vitro pri-miR-150 processing performed using extracts of wild-type or *Ksrp*$^{-/-}$ iWAT. Extracts prepared from two different wild-type and *Ksrp*$^{-/-}$ mice were used. *E*: In vitro pri-miR-150 processing performed using extracts of wild-type iWAT or *Ksrp*$^{-/-}$ iWAT in the absence or presence of recombinant KSRP. *F*: In vitro pri-miR-23b processing performed using extracts of wild-type or *Ksrp*$^{-/-}$ iWATs.

a predicted miR-150 site, and both fragments (F1 and F2) of *Ppargc1a* contain one predicted site (Fig. 6*A*). The expression of miR-150 decreased the expression of luciferase reporters harboring F2, but not F1, of *Prdm16*, and F2, but not F1, of *Ppargc1a* compared with a control miRNA (Fig. 6*B*). By contrast, miR-150 expression did not alter the expression of a control reporter (MT01) without an insertion (Fig. 6*B*). Mutations of the miR-150 target sites in F2 of *Prdm16* and F2 of *Ppargc1a* resisted inhibition by miR-150 (Fig. 6*B*). These data indicate that miR-150 directly regulates the expression of PRDM16 and PPARGC1α, leading to changes in the expression of their downstream target genes, such as *Ucp1*, *Cidea*, *Cox8b*, and *Ppara*, and suggest that the absence of KSRP leads to derepression of *Prdm16* and *Ppargc1a* through a decrease in miR-150 expression.

Downregulation of PRDM16 and PPARGC1α Attenuates Expression of Brown Fat–Selective Genes

To determine whether the increase in brown fat–selective gene expression in the absence of KSRP is due to increased expression of PRDM16 and PPARGC1α, we downregulated their expression by siRNAs in SVF cells. The downregulation of PRDM16 in wild-type and *Ksrp*$^{-/-}$ SVF cells decreased the expression of *Ucp1*, *Cidea*, *Cox8b*, *Ppargc1a*, and *Ppara*. PPARGC1α knockdown decreased the expression of *Ucp1*, *Cidea*, *Cox8b*, and *Ppara*, but not of *Prdm16*, in wild-type and *Ksrp*$^{-/-}$ SVF cells (Supplementary Fig. 5*A*

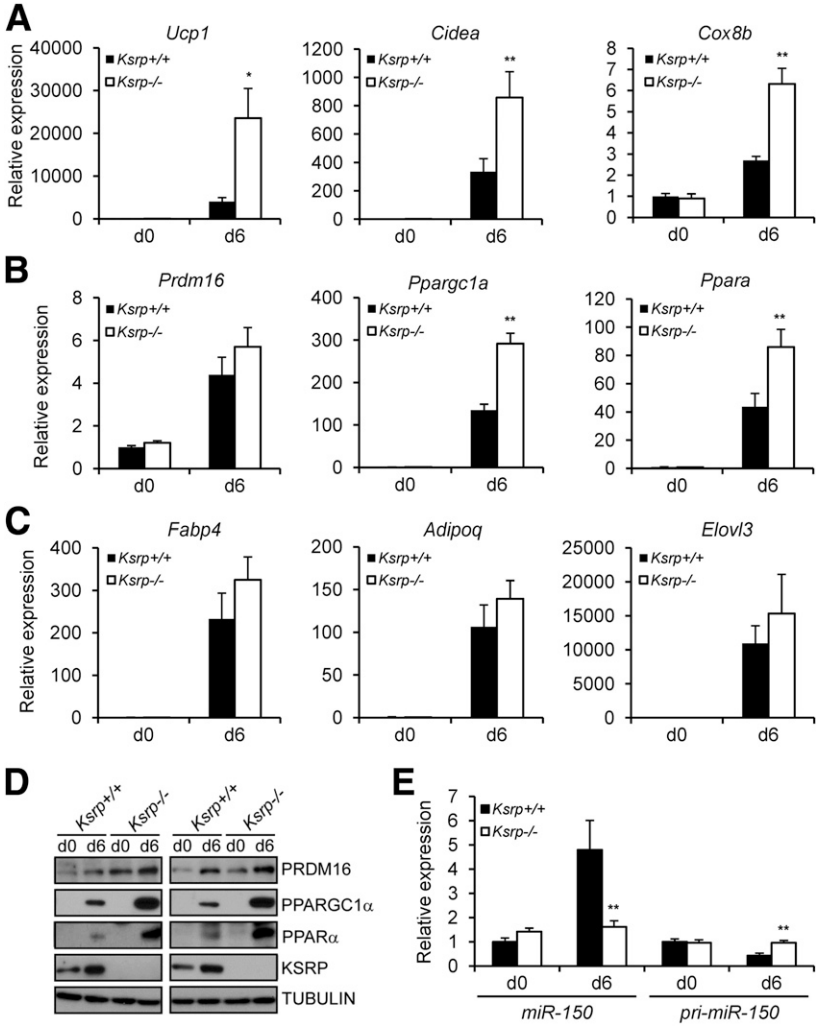

Figure 4—Elevated expression of brown fat–selective genes in differentiated SVF cells of *Ksrp*$^{-/-}$ iWAT. *A*: Wild-type and *Ksrp*$^{-/-}$ iWAT SVF cells were induced for adipocyte differentiation. Expression of *Ucp1*, *Cidea*, and *Cox8b* was analyzed by qPCR before (d0) and 6 days (d6) after differentiation. *B*: Expression of *Prdm16*, *Ppargc1a*, and *Ppara* analyzed by qPCR in SVF cells at d0 and d6 after differentiation. *C*: Expression of *Fabp4*, *Adipoq*, and *Elovl3* analyzed by qPCR in SVF cells at d0 and d6 after differentiation. *D*: Expression of PRDM16, PPARGC1α, PPARα, KSRP, and α-tubulin analyzed by immunoblotting in SVF cells at d0 and d6 after differentiation. *E*: Expression of miR-150 and pri-miR-150 analyzed by qPCR in SVF cells at d0 and d6 after differentiation. All data are represented as the mean ± SEM from three independent preparations of SVF cells. **P* < 0.05, ***P* < 0.01.

and *B*). By contrast, the downregulation of PRDM16 or PPARGC1α did not alter the expression of *Fabp4*, *Adipoq*, and *Elovl3* (Supplementary Fig. 5*C*), indicating that adipocyte differentiation was not affected under these conditions. These data strongly indicate that the increase in the brown fat gene program in the absence of KSRP is indeed due to increased expression of PRDM16 and PPARGC1α.

Elevated Expression of *miR-150* and *Ksrp* in Diet-Induced Obesity

We examined the expression of *miR-150* and *Ksrp* in a model of DIO, and found elevated expression of *miR-150* and *Ksrp* in the iWAT of wild-type mice on an HFD and reduced miR-150 levels in HFD-fed *Ksrp*$^{-/-}$ iWAT compared with HFD-fed wild-type iWAT (Fig. 7*A*). HFD feeding also increased mRNA levels of *Prdm16*, *Ppargc1a*, *Fabp4*, *Ucp1*, *Cox8b*, *Cidea*, *Dio2*, *Cpt1b*, and *Acadl* in wild-type iWAT (Fig. 7*A–D*), and levels of *Ucp1*, *Cox8b*, *Cidea*, *Cpt1b*, and *Acadl* were further upregulated in HFD-fed *Ksrp*$^{-/-}$ mice (Fig. 7*B–D*). We also detected an increase in KSRP and PPARGC1α, but not of PRDM16, in wild-type mice fed an HFD compared with a NCD, and a further upregulation of PPARGC1α and PRDM16 in HFD-fed *Ksrp*$^{-/-}$ mice (Fig. 7*E*). Since the mRNA levels of *Prdm16* and *Ppargc1a* were not elevated in HFD-fed *Ksrp*$^{-/-}$ mice compared with HFD-fed wild-type mice, we suggest that the increase in protein levels was likely due to increased translation through reduced miR-150 levels. More importantly, body weight and fad pad weights were reduced in HFD-fed *Ksrp*$^{-/-}$ mice (Fig. 7*F* and *G*). These data suggest a model in which elevated

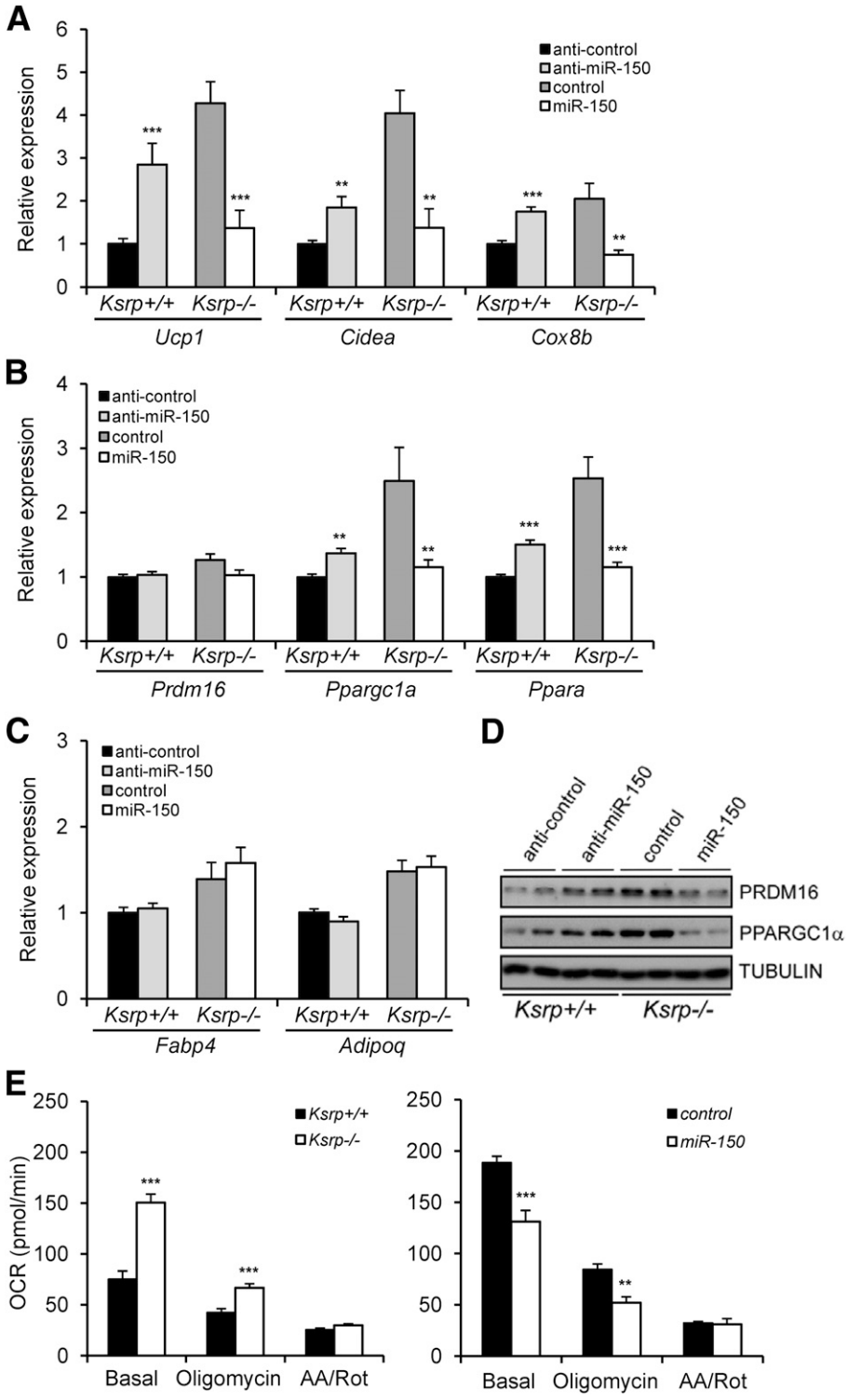

Figure 5—miR-150 regulates brown fat–selective gene expression and mitochondrial aspiration. The expression of *Ucp1*, *Cidea*, and *Cox8b* (*A*); *Prdm16*, *Ppargc1a*, and *Ppara* (*B*); and *Fabp4* and *Adipoq* (*C*) was analyzed by qPCR in wild-type SVF cells transfected with a control miRNA inhibitor or a miR-150 inhibitor, and *Ksrp*$^{-/-}$ SVF cells were transfected with a control miRNA mimic or a miR-150 mimic after 5 days of differentiation. Data are represented as the mean ± SEM from three independent preparations of SVF cells. $^{**}P < 0.01$, $^{***}P < 0.001$. *D*: Expression of PRDM16, PPARGC1α, and α-tubulin analyzed by immunoblotting in wild-type SVF cells treated with a control miRNA inhibitor or an miR-150 inhibitor and in *Ksrp*$^{-/-}$ SVF cells treated with a control miRNA mimic or an miR-150 mimic after 5 days of differentiation. Similar results were obtained using another preparation and transfection of wild-type and *Ksrp*$^{-/-}$ SVF cells. *E*: OCRs in differentiated wild-type and *Ksrp*$^{-/-}$ SVF cells (left panel) and differentiated *Ksrp*$^{-/-}$ SVF cells transfected with a control miRNA mimic or an miR-150 mimic (right panel). OCRs from untreated cells and cells treated with oligomycin and with both antimycin A and rotenone (AA/Rot) were measured and normalized with protein concentrations. The data are represented as the mean ± SEM from nine wells for each condition. $^{**}P < 0.01$, $^{***}P < 0.001$.

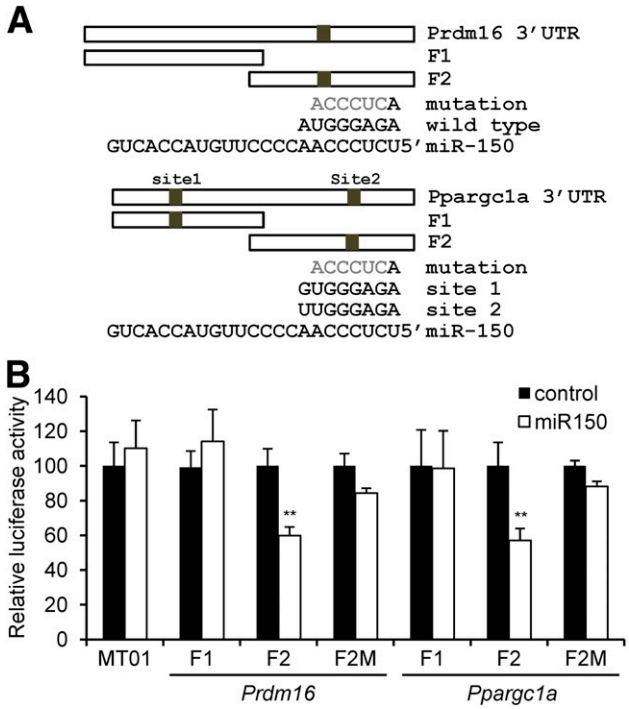

Figure 6—miR-150 directly represses *Prdm16* and *Ppargc1a*. *A*: Schematic diagrams showing 3′ UTRs of *Prdm16* and *Ppargc1a*. Two overlapping fragments (F1 and F2) from each 3′ UTR were subcloned into a dual luciferase reporter, pEZX-MT01. miR-150 target sites are indicated, and mutations in the seed motif are also denoted. *B*: Relative luciferase activities in NIH3T3 cells cotransfected with a control reporter (MT01) or reporter constructs containing F1 or F2 of *Prdm16*, mutated F2 of *Prdm16* (F2M), F1 or F2 of *Ppargc1a*, or mutated F2 of *Ppargc1a* (F2M) and a control mimic or an miR-150 mimic. Data are represented as the mean ± SEM from three independent experiments. $^{**}P < 0.01$.

expression of both KSRP and miR-150 is likely permissive for the development of obesity, and in which the absence of KSRP promotes a reduction in adiposity in DIO by enhancing brown-like transformation of iWAT through the increased expression of PPARGC1α and PRDM16.

DISCUSSION

This study shows that targeted deletion of KSRP enhances brown fat–selective gene expression in iWAT through the elevated expression of PRDM16, PPARGC1α, and PPARα, which are important regulators for the thermogenic program in BAT and for brown-like remodeling in WAT. We demonstrated that KSRP is involved in the processing of pri-miR-150 in iWAT and its absence results in downregulation of miR-150. Mechanistically, miR-150 directly represses *Prdm16* and *Ppargc1a* expression. Thus, reduction in miR-150 levels in *Ksrp*$^{-/-}$ iWAT leads to elevated expression of PRDM16 and PPARGC1α, thereby increasing the brown fat gene program. In addition, we also found increased expression of fatty acid oxidation genes in *Ksrp*$^{-/-}$ iWAT, likely due to the upregulation of PPARGC1α and PPARα, which are critical regulators for enhancing fatty acid use (38–40). The expression of brown fat–selective and fatty acid oxidation genes in the eWAT of *Ksrp*$^{-/-}$ mice was also increased. By contrast, KSRP ablation did not alter the brown fat gene program in BAT, likely due to a lower expression of KSRP and miR-150 in BAT. These findings suggest that KSRP is a critical factor for balancing energy storage and EE in white adipocytes, and its absence favors EE, partly through post-transcriptional regulation of miR-150 expression.

Targeted deletion of *miR-150* leads to B-cell expansion and an enhanced humoral immune response due to c-Myb upregulation (41). The body weight and fat mass of *Mir150*$^{-/-}$ mice compared with wild-type mice were not reported. Consistent with the observation with HFD feeding (Fig. 7*A*), miR-150 was also reported to be upregulated in subcutaneous adipose tissue of obese human subjects (42). While *Ppargc1a* was predicted to be a target of miR-150, its levels were not altered in obese adipose tissue (42). Using adipocytes derived from SVF cells of iWAT, we demonstrate that ectopic expression of miR-150 attenuates *Prdm16*, *Ppargc1a*, and *Ppara* expression, and, conversely, that the inhibition of miR-150 expression increases their expression. Although *Prdm16* and *Ppargc1a* are directly targeted by miR-150, *Ppara* does not contain any predicted target site. The regulation of *Ppara* expression by miR-150 is likely indirect due to the altered expression of *Prdm16* and *Ppargc1a* (see below). Our results point to miR-150 as a negative regulator of inducible brown-like adipocytes in iWAT by repressing *Prdm16* and *Ppargc1a*.

PRDM16 is a determinant of brown fat lineage and is able to induce browning of subcutaneous WAT (8,12,13). PPARGC1α is recognized as a critical regulator of thermogenesis and oxidative metabolism (43). PPARα is also critical for the expression of brown fat and fatty acid oxidation genes in BAT (44). We found that PRDM16 knockdown in SVF cells attenuated the expression of *Ppargc1a*, *Ppara*, and brown fat markers, and that PPARGC1α knockdown decreased the expression of *Ppara,* but not of *Prdm16,* and brown fat markers (Supplementary Fig. 5). These results strongly suggest that the enhanced brown-like transformation in *Ksrp*$^{-/-}$ iWAT at least in part results from the elevated expression of *Prdm16*, *Ppargc1a*, and *Ppara*. These data are also consistent with previous studies showing that PRDM16 lines upstream of PPARGC1α and PPARα (8,25,45), and that PRDM16 and PPARGC1α are positive regulators for brown fat gene expression (8,17). While it was shown that PPARα activates *Ppargc1a* expression through coactivation by PRDM16 (46), our data suggest that PPARGC1α also regulates *Ppara* expression. Thus, there is a mutual regulation between PPARGC1α and PPARα.

While *Ksrp*$^{-/-}$ mice have reduced fat mass and increased EE, it will be of interest to see whether the enhanced brown fat gene program in iWAT is the sole contribution to these phenotypes. Using mice with both

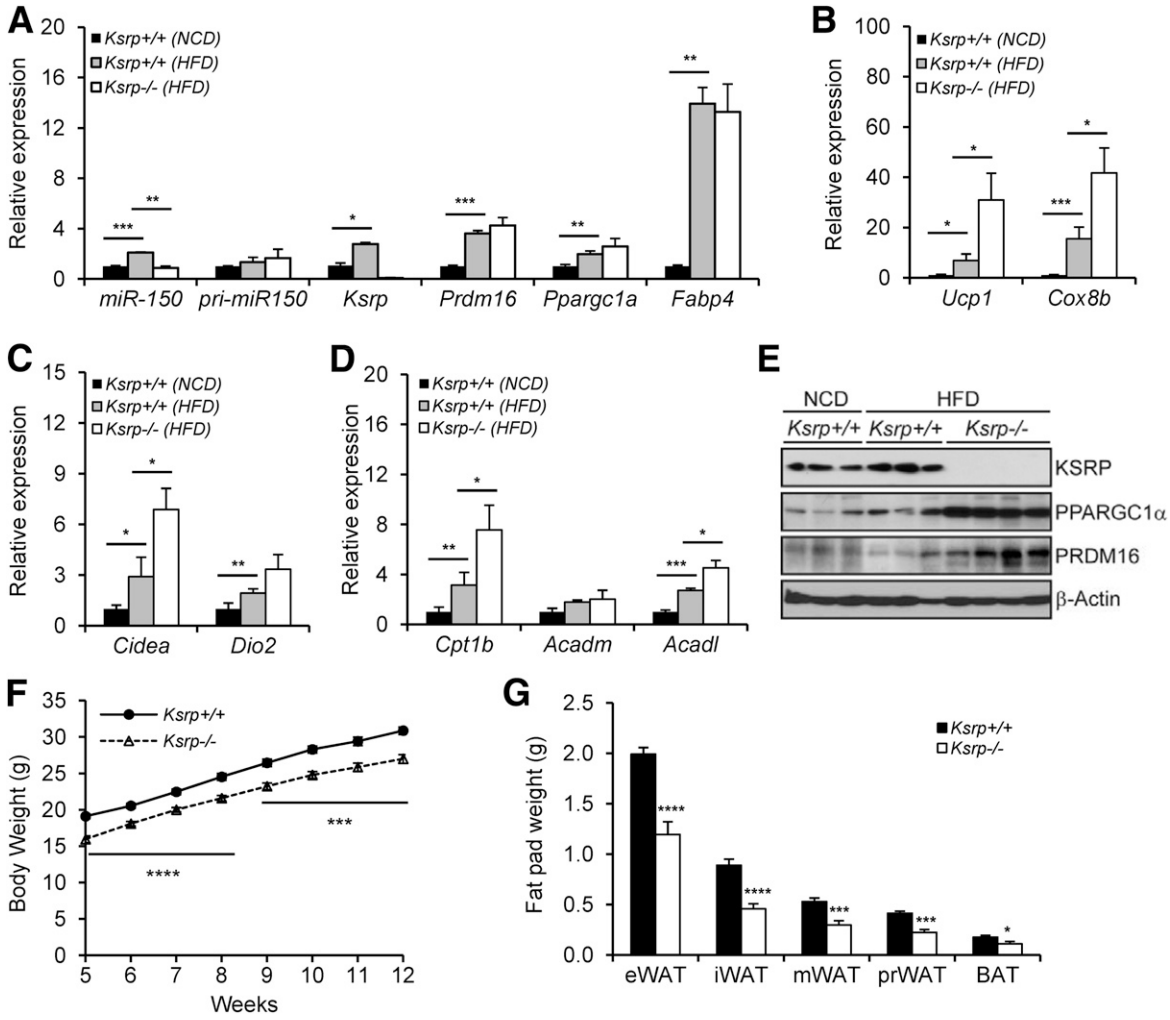

Figure 7—HFD feeding increases the expression of *miR-150* and *Ksrp*, and KSRP ablation reduces adiposity in DIO. The expression of *miR-150*, *pri-miR-150*, *Ksrp*, *Prdm16*, *Ppargc1a*, and *Fabp4* (*A*); *Ucp1* and *Cox8b* (*B*); *Cidea* and *Dio2* (*C*); and *Cpt1b*, *Acadm*, and *Acadl* (*D*) in wild-type mice (n = 8) fed a NCD and wild-type (n = 7) and $Ksrp^{-/-}$ (n = 7) mice fed an HFD. *E*: Expression of KSRP, PPARGC1α, PRDM16, and β-actin in wild-type mice fed a NCD and wild-type and $Ksrp^{-/-}$ mice fed an HFD. *F*: Body weights of wild-type (n = 10) and $Ksrp^{-/-}$ male mice (n = 10) fed an HFD from week 5 to week 12. *G*: Fat pad weights of 14-week-old wild-type (n = 10) and $Ksrp^{-/-}$ (n = 10) male mice fed an HFD. All data are represented as the mean ± SEM. *P < 0.05, **P < 0.01, ***P < 0.001, ****P < 0.0001. mWAT, mesenteric WAT; prWAT, perirenal WAT.

KSRP ablation and adipose-specific overexpression of miR-150 should provide an answer. Furthermore, since our mouse model is a global KSRP knockout, other effects on lipid metabolism in metabolic tissues, such as muscle and liver, may also contribute to the observed leanness. Further studies using adipose-specific KSRP knock-out mice should reveal additional functions of KSRP in controlling whole-body adiposity and lipid metabolism. Nevertheless, our observations in $Ksrp^{-/-}$ mice are consistent with a large body of previous studies (8–11,21,24,47–52) revealing that increasing the browning of WAT shows resistance to DIO and improved glucose metabolism. In summary, this work demonstrates the in vivo role of KSRP in post-transcriptional regulation of miRNA expression to control brown-like remodeling of iWAT, and suggests that modulation of KSRP-dependent pri-miR-150 processing could potentially lead to therapeutics for obesity and metabolic disorders.

Acknowledgments. The authors thank Dr. Maria S. Johnson, University of Alabama at Birmingham, Animal Models Core, for conducting body composition analysis and indirect calorimetry; Dr. Martin Young, University of Alabama at Birmingham, for metabolic analysis using the Comprehensive Lab Animal Monitoring System; Dr. Chih-Hsuan Wang, Auburn University, for biostatistics analysis; and Dr. Douglas Moellering, University of Alabama at Birmingham-Comprehensive Diabetes Center, Core Diabetes Research Center Redox Biology Core (supported by National Institutes of Health grant P60 DK079626), for advice on and design of the measurement of oxygen consumption rates.

Funding. This work was supported by grants from Ministero della Salute (RF-2010-2306205) and the Association for International Cancer Research (#10-0527) to R.G., and by National Institutes of Health grant GM068758 (C.-Y.C.).

Duality of Interest. No potential conflicts of interest relevant to this article were reported.

Author Contributions. C.-F.C. helped to design and performed the experiments, analyzed the data, and wrote the manuscript. Y.-Y.L., H.-K.W., X.Z., M.G., P.B., and R.G. performed the experiments and analyzed the data. W.T.G. helped to conceive the project. C.-Y.C. helped to conceive the project and to design the experiments. C.-Y.C. is the guarantor of this work and, as such, had full access to all the data in the study and takes responsibility for the integrity of the data and the accuracy of the data analysis.

References

1. Cannon B, Nedergaard J. Brown adipose tissue: function and physiological significance. Physiol Rev 2004;84:277–359
2. Cypess AM, Lehman S, Williams G, et al. Identification and importance of brown adipose tissue in adult humans. N Engl J Med 2009;360:1509–1517
3. van Marken Lichtenbelt WD, Vanhommerig JW, Smulders NM, et al. Cold-activated brown adipose tissue in healthy men. N Engl J Med 2009;360:1500–1508
4. Farmer SR. Obesity: be cool, lose weight. Nature 2009;458:839–840
5. Cousin B, Cinti S, Morroni M, et al. Occurrence of brown adipocytes in rat white adipose tissue: molecular and morphological characterization. J Cell Sci 1992;103:931–942
6. Ghorbani M, Himms-Hagen J. Appearance of brown adipocytes in white adipose tissue during CL 316,243-induced reversal of obesity and diabetes in Zucker fa/fa rats. Int J Obes Relat Metab Disord 1997;21:465–475
7. Barbatelli G, Murano I, Madsen L, et al. The emergence of cold-induced brown adipocytes in mouse white fat depots is determined predominantly by white to brown adipocyte transdifferentiation. Am J Physiol Endocrinol Metab 2010;298:E1244–E1253
8. Seale P, Conroe HM, Estall J, et al. Prdm16 determines the thermogenic program of subcutaneous white adipose tissue in mice. J Clin Invest 2011;121:96–105
9. Cederberg A, Grønning LM, Ahrén B, Taskén K, Carlsson P, Enerbäck S. FOXC2 is a winged helix gene that counteracts obesity, hypertriglyceridemia, and diet-induced insulin resistance. Cell 2001;106:563–573
10. Leonardsson G, Steel JH, Christian M, et al. Nuclear receptor corepressor RIP140 regulates fat accumulation. Proc Natl Acad Sci U S A 2004;101:8437–8442
11. Qiang L, Wang L, Kon N, et al. Brown remodeling of white adipose tissue by SirT1-dependent deacetylation of Pparγ. Cell 2012;150:620–632
12. Kajimura S, Seale P, Kubota K, et al. Initiation of myoblast to brown fat switch by a PRDM16-C/EBP-beta transcriptional complex. Nature 2009;460:1154–1158
13. Seale P, Bjork B, Yang W, et al. PRDM16 controls a brown fat/skeletal muscle switch. Nature 2008;454:961–967
14. Boström P, Wu J, Jedrychowski MP, et al. A PGC1-α-dependent myokine that drives brown-fat-like development of white fat and thermogenesis. Nature 2012;481:463–468
15. Fisher FM, Kleiner S, Douris N, et al. FGF21 regulates PGC-1α and browning of white adipose tissues in adaptive thermogenesis. Genes Dev 2012;26:271–281
16. Vernochet C, Peres SB, Davis KE, et al. C/EBPalpha and the corepressors CtBP1 and CtBP2 regulate repression of select visceral white adipose genes during induction of the brown phenotype in white adipocytes by peroxisome proliferator-activated receptor gamma agonists. Mol Cell Biol 2009;29:4714–4728
17. Puigserver P, Wu Z, Park CW, Graves R, Wright M, Spiegelman BM. A cold-inducible coactivator of nuclear receptors linked to adaptive thermogenesis. Cell 1998;92:829–839
18. Powelka AM, Seth A, Virbasius JV, et al. Suppression of oxidative metabolism and mitochondrial biogenesis by the transcriptional corepressor RIP140 in mouse adipocytes. J Clin Invest 2006;116:125–136
19. Picard F, Géhin M, Annicotte J, et al. SRC-1 and TIF2 control energy balance between white and brown adipose tissues. Cell 2002;111:931–941
20. Hansen JB, Jørgensen C, Petersen RK, et al. Retinoblastoma protein functions as a molecular switch determining white versus brown adipocyte differentiation. Proc Natl Acad Sci U S A 2004;101:4112–4117
21. Scimè A, Grenier G, Huh MS, et al. Rb and p107 regulate preadipocyte differentiation into white versus brown fat through repression of PGC-1alpha. Cell Metab 2005;2:283–295
22. Trajkovski M, Ahmed K, Esau CC, Stoffel M. MyomiR-133 regulates brown fat differentiation through Prdm16. Nat Cell Biol 2012;14:1330–1335
23. Yin H, Pasut A, Soleimani VD, et al. MicroRNA-133 controls brown adipose determination in skeletal muscle satellite cells by targeting Prdm16. Cell Metab 2013;17:210–224
24. Mori M, Nakagami H, Rodriguez-Araujo G, Nimura K, Kaneda Y. Essential role for miR-196a in brown adipogenesis of white fat progenitor cells. PLoS Biol 2012;10:e1001314
25. Sun L, Xie H, Mori MA, et al. Mir193b-365 is essential for brown fat differentiation. Nat Cell Biol 2011;13:958–965
26. Chen Y, Siegel F, Kipschull S, et al. miR-155 regulates differentiation of brown and beige adipocytes via a bistable circuit. Nat Commun 2013;4:1769
27. Min H, Turck CW, Nikolic JM, Black DL. A new regulatory protein, KSRP, mediates exon inclusion through an intronic splicing enhancer. Genes Dev 1997;11:1023–1036
28. Gherzi R, Lee KY, Briata P, et al. A KH domain RNA binding protein, KSRP, promotes ARE-directed mRNA turnover by recruiting the degradation machinery. Mol Cell 2004;14:571–583
29. Trabucchi M, Briata P, Garcia-Mayoral M, et al. The RNA-binding protein KSRP promotes the biogenesis of a subset of microRNAs. Nature 2009;459:1010–1014
30. Dhamija S, Kuehne N, Winzen R, et al. Interleukin-1 activates synthesis of interleukin-6 by interfering with a KH-type splicing regulatory protein (KSRP)-dependent translational silencing mechanism. J Biol Chem 2011;286:33279–33288
31. Chen CY, Gherzi R, Ong SE, et al. AU binding proteins recruit the exosome to degrade ARE-containing mRNAs. Cell 2001;107:451–464
32. Lin WJ, Zheng X, Lin CC, et al. Posttranscriptional control of type I interferon genes by KSRP in the innate immune response against viral infection. Mol Cell Biol 2011;31:3196–3207
33. Soukas A, Socci ND, Saatkamp BD, Novelli S, Friedman JM. Distinct transcriptional profiles of adipogenesis in vivo and in vitro. J Biol Chem 2001;276:34167–34174
34. Fine JB, DiGirolamo M. A simple method to predict cellular density in adipocyte metabolic incubations. Int J Obes Relat Metab Disord 1997;21:764–768
35. Briata P, Lin WJ, Giovarelli M, et al. PI3K/AKT signaling determines a dynamic switch between distinct KSRP functions favoring skeletal myogenesis. Cell Death Differ 2012;19:478–487
36. Pasero M, Giovarelli M, Bucci G, Gherzi R, Briata P. Bone morphogenetic protein/SMAD signaling orients cell fate decision by impairing KSRP-dependent microRNA maturation. Cell Rep 2012;2:1159–1168
37. Hall MP, Huang S, Black DL. Differentiation-induced colocalization of the KH-type splicing regulatory protein with polypyrimidine tract binding protein and the c-src pre-mRNA. Mol Biol Cell 2004;15:774–786
38. Lin J, Handschin C, Spiegelman BM. Metabolic control through the PGC-1 family of transcription coactivators. Cell Metab 2005;1:361–370
39. Finck BN, Kelly DP. PGC-1 coactivators: inducible regulators of energy metabolism in health and disease. J Clin Invest 2006;116:615–622
40. Lefebvre P, Chinetti G, Fruchart JC, Staels B. Sorting out the roles of PPAR alpha in energy metabolism and vascular homeostasis. J Clin Invest 2006;116:571–580
41. Xiao C, Calado DP, Galler G, et al. MiR-150 controls B cell differentiation by targeting the transcription factor c-Myb. Cell 2007;131:146–159
42. Martinelli R, Nardelli C, Pilone V, et al. miR-519d overexpression is associated with human obesity. Obesity (Silver Spring) 2010;18:2170–2176

43. Wu Z, Puigserver P, Andersson U, et al. Mechanisms controlling mitochondrial biogenesis and respiration through the thermogenic coactivator PGC-1. Cell 1999; 98:115–124

44. Ahmadian M, Abbott MJ, Tang T, et al. Desnutrin/ATGL is regulated by AMPK and is required for a brown adipose phenotype. Cell Metab 2011;13:739–748

45. Seale P, Kajimura S, Yang W, et al. Transcriptional control of brown fat determination by PRDM16. Cell Metab 2007;6:38–54

46. Hondares E, Rosell M, Díaz-Delfín J, et al. Peroxisome proliferator-activated receptor α (PPARα) induces PPARγ coactivator 1α (PGC-1α) gene expression and contributes to thermogenic activation of brown fat: involvement of PRDM16. J Biol Chem 2011;286:43112–43122

47. Polak P, Cybulski N, Feige JN, Auwerx J, Rüegg MA, Hall MN. Adipose-specific knockout of raptor results in lean mice with enhanced mitochondrial respiration. Cell Metab 2008;8:399–410

48. Tsukiyama-Kohara K, Poulin F, Kohara M, et al. Adipose tissue reduction in mice lacking the translational inhibitor 4E-BP1. Nat Med 2001;7:1128–1132

49. Romanatto T, Roman EA, Arruda AP, et al. Deletion of tumor necrosis factor-alpha receptor 1 (TNFR1) protects against diet-induced obesity by means of increased thermogenesis. J Biol Chem 2009;284:36213–36222

50. Singh R, Xiang Y, Wang Y, et al. Autophagy regulates adipose mass and differentiation in mice. J Clin Invest 2009;119:3329–3339

51. Toh SY, Gong J, Du G, et al. Up-regulation of mitochondrial activity and acquirement of brown adipose tissue-like property in the white adipose tissue of fsp27 deficient mice. PLoS One 2008;3:e2890

52. Lodhi IJ, Yin L, Jensen-Urstad AP, et al. Inhibiting adipose tissue lipogenesis reprograms thermogenesis and PPARγ activation to decrease diet-induced obesity. Cell Metab 2012;16:189–201